**Communications in Mathematics and Applications**
Vol. 16, No. 4, pp. 1077–1091, 2025
ISSN 0975-8607 (online); 0976-5905 (print)
Published by RGN Publications
DOI: 10.26713/cma.v16i4.3267

http://www.rgnpublications.com

Research Article

# Lucas Wavelet Analysis of the Squeeze Film Characteristics Between a Sphere and a Flat Plate of Couple Stress Fluid Model

S. C. Shiralashetti*, A. M. Sangolli and N. T. Vatsala

*Department of Mathematics, Karnatak University, Dharwad 580003, Karnataka, India*
***Corresponding author:** scshiralashetti@kud.ac.in

**Received:** July 4, 2025 **Revised:** August 9, 2025 **Accepted:** August 20, 2025

**Abstract.** This study presents a numerical examination of the influence of couple stresses on the squeeze film behavior between a sphere and a flat plate, grounded in microcontinuum theory. The revised Reynolds equation that regulates the squeezing film pressure is formulated by employing the Stokes constitutive equations to incorporate the couple stress effects resulting from the lubricant mixed with distinct additives. Lucas wavelet based numerical scheme is developed for the numerical solution of the governing modified Reynolds equation. The numerical solution indicates that the presence of couple stresses results in an increase in the film pressure. Overall, the effects of couple stress, as defined by the couple stress parameter, lead to an enhancement in the load-carrying capacity when compared to the traditional Newtonian-lubricant scenario. The characteristics of the squeeze film in the system are enhanced.

**Keywords.** Lucas wavelet, Squeeze film, Couple stress fluid model, Microcontinuum theory, Sphere and plate

**Mathematics Subject Classification (2020).** 76D08, 65Txx, 34Bxx



## 1. Introduction

The investigation into *Squeeze Film* (SF) characteristics has garnered significant attention due to its extensive applications in engineering fields, including gyroscopes, bearings, gears, aircraft engines, automotive engines, machine tools, rolling elements, attitude control devices, and

skeletal joints. Traditionally, analysis of SF performance assumes that the lubricant behaves fundamentally like a Newtonian viscous fluid. Numerous researchers have examined the SF performance utilizing the Newtonian lubricants (Burbidge and Servais [3], and Jackson [11]). The application of various liquids as lubricants in diverse conditions has become increasingly significant with the advancement of modern machinery. Since the non-Newtonian behaviour of oils with polymeric additions cannot be explained by the conventional continuum theory, the micro-continuum theory is derived from the non-polar theory to take into consideration the inherent motion of material constituents (Ariman *et al*. [1], and Gupta and Gupta [9]). The *Couple Stress* (CS) theory of fluids, developed by Stokes [23], represents the most straightforward extension of classical fluid theory, accommodating polar effects including body couples, non-symmetric tensors, and couple stresses. The purpose of this CS fluid model is to account for additive particle-size effects. Naduvinamani *et al*. [17] studied the squeeze film journal bearings, and they found that the presence of microstructures in the fluid film causes an enhancement of squeeze-film pressure and hence an increase in the load-carrying capacity. Lu and Lin [14] investigated the SF properties in the sphere-plate configuration and determined that these characteristics are enhanced, particularly at elevated values of the CS parameter and viscosity parameter. Hashimoto [10] investigated the fluctuation in pressure distribution over time for various fluids between two parallel circular plates under sinusoidal squeeze motion. The investigation of CS characteristics in porous parallel stepped plates demonstrated that the presence of CS significantly increases the SF pressure and load-carrying capability, while simultaneously reducing the response time in comparison with the classical Newtonian lubricant case. Furthermore, the study of Biradar [2] indicated that an increase in step height leads to a decline in load-carrying capability.

Several numerical methods exist for solving initial and boundary value problems associated with *Ordinary Differential Equations* (ODEs). Among the most widely used are the *Finite Difference Method* (FDM), the *Finite Element Method* (FEM), and the boundary integral equation method (Fox [7], Gerald and Wheatley [8], and Reddy [20]). In recent decades, wavelets have captured the attention of numerous scholars because of their effectiveness in solving differential equations with remarkable accuracy and reduced computational effort (Mehandiratta *et al*. [16], and Torrence and Compo [24]). The most straightforward of these is the Haar wavelet is used to solve the ODE (Lu and Lin [14], and Mai-Duy and Tran-Cong [15]). Shiralashetti *et al*. [22] used the Jacobi wavelets for the solution of the laminar nanofluid flow problem. The Daubechies Wavelet Multigrid Method is employed to address the Hydrodynamic Lubrication problem (Shiralashetti *et al*. [21]). Modified Lucas wavelets for the approximate solutions of initial and boundary value problems (Kumar [12]). Kumbinarasaiah *et al*. [13] resolve the nanofluid's magnetohydrodynamic boundary layer flow issue, with the help of the Bernoulli wavelet based numerical method. *Lucas Wavelet Operational Matrix Method* (LWOMM) is developed for the analysis of the SF characteristics between a sphere and a flat plate with the help of CS fluid model in this study. This article is structured as follows. Preliminaries of Lucas wavelet and the lubrication problem in Section 2. Section 3 is devoted to the LWOMM of the solution. The implementation of LWOMM is outlined in Section 4. Section 5 presents the findings and analyses. Finally, the conclusion is described in Section 6.

## 2. Preliminaries of Lucas Wavelet

The mother wavelet, often simply called a wavelet, generates a family of functions through scaling (dilating) and shifting (translating) a single function $\Psi$. When the scaled parameter $\chi$ and shift parameter $\xi$ change continuously, they produce a continuous family of wavelets $\Psi_{\chi,\xi}(\theta)$ is as follows [19],

$$\Psi_{\chi,\xi}(\theta) = (\chi)^{-\frac{1}{2}}\Psi\left(\frac{\theta-\xi}{\chi}\right), \quad \chi,\xi \in R,\ \xi \neq 0. \tag{2.1}$$

By limiting the parameters $\chi$ and $\xi$ to specific discrete values, namely, setting $\chi = \chi_0^k$, and$\xi = \alpha\xi_0\chi_0^k$, where $\chi_0 > 1$, $\xi_0 > 1$, $\alpha$, and $k$ are positive integers, we obtain a corresponding family of discrete wavelets,

$$\Psi_{k,\alpha}(\theta) = (\chi_0)^{\frac{k}{2}}\Psi(\chi_0^k\theta - \alpha\xi_0), \tag{2.2}$$

where $\Psi_{k,\alpha}(\theta)$ constitute a wavelet basis for $L^2(R)$.

We now define the *Lucas Wavelet* (LW) $\Psi_{\alpha,\beta}(\theta) = \Psi(\alpha,k,\beta,\theta)$, which depends on four parameters, $\alpha = 1,2,\ldots,2^{k-1}$, $k$ is any positive integer, $\beta$ represents the order of the Lucas polynomials, and $\theta$denotes the normalized time. Accordingly, the Lucas wavelet is defined on the interval $[0,1)$ as follows [6],

$$\Psi_{\alpha,\beta}(\theta) = \begin{cases} 2^{\frac{k-1}{2}}\Im_\beta(2^{k-1}\theta - \alpha + 1), & \frac{\alpha-1}{2^{k-1}} \leq \theta < \frac{\alpha}{2^{k-1}}, \\ 0, & \text{otherwise}, \end{cases} \tag{2.3}$$

where $\beta = 0,1,2,\ldots,m$, $\Im_\beta(2^{k-1}\theta - \alpha + 1) = \frac{1}{\sqrt{\int_0^1 L_\beta^2(\theta)d\theta}}L_\beta(2^{k-1}\theta - \alpha + 1)$. The $L_\beta(\theta)$ denotes the Lucas polynomial of degree $\beta$, defined on the interval $[0,1]$, as follows [18],

$$L_0(\theta) = 2,\ L_\beta(\theta) = \sum_{\lambda=0}^{\left[\frac{\beta}{2}\right]} \frac{\beta}{\beta-\lambda}\binom{\beta-\lambda}{k}\theta^{\beta-2\lambda}, \quad \beta > 0. \tag{2.4}$$

A function $g$ defined on the interval $[0,1)$ can be expressed using LWs in the following way:

$$g(\theta) = \sum_{\alpha=1}^{\infty}\sum_{\beta=0}^{\infty} A_{\alpha,\beta}\Psi_{\alpha,\beta}(\theta).$$

The following is a truncation of the infinite series mentioned above:

$$g(\theta) \simeq \sum_{\alpha=1}^{2^{k-1}}\sum_{\beta=0}^{\Upsilon} A_{\alpha,\beta}\Psi_{\alpha,\beta}(\theta) = B^T\Psi(\theta), \tag{2.5}$$

where

$$B = [A_{1,0}, A_{1,1}, \ldots, A_{1,\Upsilon}, \ldots A_{2^{k-1},0}, A_{2^{k-1},1}, \ldots A_{2^{k-1},\Upsilon}]^T$$

and

$$\Psi(\theta) = [\Psi_{1,0}(\theta), \Psi_{1,1}(\theta), \ldots, \Psi_{1,\Upsilon}(\theta), \ldots, \Psi_{2^{k-1},0}(\theta), \Psi_{2^{k-1},1}(\theta), \ldots, \Psi_{2^{k-1},\Upsilon}(\theta)]^T.$$

Thus, each component of the vector $B$ is derived from the following relation:

$$A_{\alpha,\beta} = \langle g(\theta), \Psi_{\alpha,\beta}(\theta)\rangle, \quad \beta = 0,1,\ldots,\Upsilon,\ \alpha = 0,1,\ldots,2^{k-1}.$$

### 2.1 Lucas Wavelet Integration Operational Matrices

In this part, the LW integration operational matrices needed to solve DEs are determined. The integration operation matrix of a specified order $N = 6$ ($\Upsilon = 2$ and $k = 2$) is initially derived.

The subsequent six LW bases are examined,

$$\Psi_{1,0}(\theta)=\begin{cases}\frac{\sqrt{2}}{2}, & 0\le\theta<\frac{1}{2},\\ 0, & \text{otherwise},\end{cases}$$

$$\Psi_{1,1}(\theta)=\begin{cases}\frac{6\sqrt{2}\theta}{2}, & 0\le\theta<\frac{1}{2},\\ 0, & \text{otherwise},\end{cases},$$

$$\Psi_{1,2}(\theta)=\begin{cases}\frac{15\sqrt{2}(4\theta^2+2)}{83}, & 0\le\theta<\frac{1}{2},\\ 0, & \text{otherwise},\end{cases}$$

$$\Psi_{2,0}(\theta)=\begin{cases}\frac{\sqrt{2}}{2}, & \frac{1}{2}\le\theta<1,\\ 0, & \text{otherwise},\end{cases},$$

$$\Psi_{2,1}(\theta)=\begin{cases}3\sqrt{2}(2\theta-1), & \frac{1}{2}\le\theta<1,\\ 0, & \text{otherwise},\end{cases}$$

$$\Psi_{2,2}(\theta)=\begin{cases}\frac{15\sqrt{2}(2+(2\theta-1)^2)}{83}, & \frac{1}{2}\le\theta<1,\\ 0, & \text{otherwise}.\end{cases} \tag{2.6}$$

The following results are obtained by integrating the wavelet basis stated in eqn. (2.6),

$$\int_0^\theta \Psi_{1,0}(\theta)d\theta=[0.0000,0.2887,0.0000,0.5000,0.0000,0.0000]^T\Psi_6(\theta),$$

$$\int_0^\theta \Psi_{1,1}(\theta)d\theta=[-0.8660,0.0000,1.0186,0.4330,0.0000,0.0000]^T\Psi_6(\theta),$$

$$\int_0^\theta \Psi_{1,2}(\theta)d\theta=[-0.2076,0.2193,0.2500,0.4960,0.0000,0.0000]^T\Psi_6(\theta),$$

$$\int_0^\theta \Psi_{2,0}(\theta)d\theta=[0.0000,0.0000,0.0000,0.0000,0.2887,0.0000]^T\Psi_6(\theta),$$

$$\int_0^\theta \Psi_{2,1}(\theta)d\theta=[0.0000,0.0000,0.0000,-0.8660,0.0000,1.0186]^T\Psi_6(\theta),$$

$$\int_0^\theta \Psi_{2,2}(\theta)d\theta=[0.0000,0.0000,0.0000,-0.2076,0.2193,0.2500]^T\Psi_6(\theta).$$

Thus,

$$\int_0^\theta \Psi(\theta)d\theta=\mathbb{Q}_{i,1}\Psi(\theta),$$

$$\mathbb{Q}_{i,1}=\begin{bmatrix} 0.0000 & 0.2887 & 0.0000 & 0.5000 & 0.0000 & 0.0000\\ -0.8660 & 0.0000 & 1.0186 & 0.4330 & 0.0000 & 0.0000\\ -0.2076 & 0.2193 & 0.2500 & 0.4960 & 0.0000 & 0.0000\\ 0.0000 & 0.0000 & 0.0000 & 0.0000 & 0.2887 & 0.0000\\ 0.0000 & 0.0000 & 0.0000 & -0.8660 & 0.0000 & 1.0186\\ 0.0000 & 0.0000 & 0.0000 & -0.2076 & 0.2193 & 0.2500\end{bmatrix} \tag{2.7}$$

is the LW integration operation matrix. Likewise, a double integration of the LW basis yields the operational matrices $\mathbb{Q}_{i,1}$, as shown below:

$$\int_0^\theta\int_0^\theta \Psi(\theta)d\theta=\mathbb{Q}_{i,2}\Psi(\theta) \text{ and } W_{i,1}=\int_0^1 \Psi(\theta)d\theta,$$

$$\mathbb{Q}_{i,2} = \begin{bmatrix} -0.2500 & 0.0000 & 0.0000 & 0.5000 & 0.0000 & 0.0000 \\ -0.0266 & -0.0266 & 0.2546 & 0.0722 & 0.1250 & 0.0000 \\ -0.2402 & -0.0045 & 0.2836 & 0.1151 & 0.1432 & 0.0000 \\ 0.0000 & 0.0000 & 0.0000 & -0.2500 & 0.0000 & 0.2940 \\ 0.0000 & 0.0000 & 0.0000 & -0.2115 & -0.0266 & 0.2546 \\ 0.0000 & 0.0000 & 0.0000 & -0.2402 & -0.0045 & 0.2836 \end{bmatrix}. \tag{2.8}$$

## 2.2 Lubrication Problem

Consider the SF mechanism depicted in Figure 1, where a rigid sphere with a radius $r$ moves towards an infinite plate at a constant velocity, subjected to a steady load.

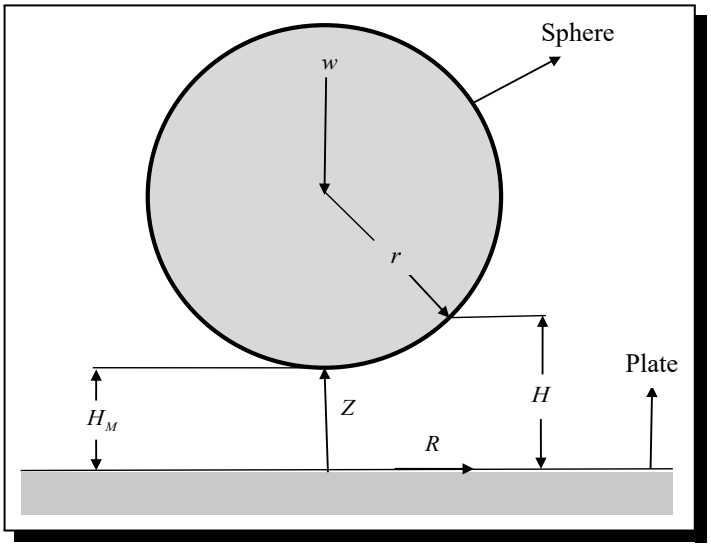


**Figure 1.** Squeeze-film interaction between a sphere and a flat surface

The lubricant used in this system is assumed to be a Stokes CS fluid. Assuming that the fluid film is thin, the fluid inertia is negligible, and no body couples or body forces are acting on the system, the momentum equations and the continuity equation governing the lubricant's motion, expressed in polar coordinates, simplify to the following form,

$$\frac{\partial P}{\partial R} = \mu \frac{\partial^2 U}{\partial Z^2} - \eta \frac{\partial^4 U}{\partial Z^4}, \tag{2.9}$$

$$\frac{\partial P}{\partial Z} = 0, \tag{2.10}$$

$$\frac{1}{R}\frac{\partial (RU)}{\partial R} + \frac{\partial W}{\partial Z} = 0. \tag{2.11}$$

The velocity component has the following *boundary conditions* (Bcs) at the plate and sphere surfaces:

$$\text{at } Z = 0; \quad \frac{\partial^2 U}{\partial Z^2} = 0, \quad W = 0, \tag{2.12}$$

and

$$\text{at } Z = h; \quad \frac{\partial^2 U}{\partial Z^2} = 0, \quad W = \frac{\partial h}{\partial t}, \tag{2.13}$$

where the oil film thickness, given that $r \gg R$, is

$$h = h_M + \frac{R^2}{2r}. \tag{2.14}$$

The expression $U$ can be obtained by integrating equation (2.9) using the aforementioned constraints,

$$U = \frac{1}{2\mu}\frac{\partial P}{\partial R}\left\{Z^2 - Zh + 2L^2\left[1 - \frac{\cosh\left(2Z - \frac{h}{2L}\right)}{\cosh\left(\frac{h}{2L}\right)}\right]\right\}, \tag{2.15}$$

where $L = \sqrt{\left(\frac{\eta}{\mu}\right)}$.

Integrate the continuity equation (2.11) with respect to $Z$ using the Bc's of $U$. The Reynolds equation, determining film pressure is derived as follows:

$$\frac{1}{R}\frac{\partial}{\partial R}\left[F(h,L)R\frac{\partial P}{\partial R}\right] = 12\mu\frac{\partial h}{\partial t} \tag{2.16}$$

where $F(h,L) = h^3 - 12L^2h + 24L^3\tanh\left(\frac{h}{2L}\right)$.

## 3. Lucas Wavelet Operational Matrix Method of Solution

We assume that the second-order ODE can be expressed by the Lucas wavelet series is given as:

$$y''(t) = \sum_{i=1}^{2^{k-1}m} a_i h_i(t). \tag{3.1}$$

According to the Bc's, equation (3.1) is twice integrated from 0 to $t$. Thus, the Lucas functions and their integrals are used to define the solution of $y(t)$ together with their derivatives $y'(t)$, and $y''(t)$. We consider the collocation points

$$t_c = \frac{c - 0.5}{2^{k-1}m}, \quad c = 1,2,\ldots,2^{k-1}m. \tag{3.2}$$

Consider the Bc's as

$$y'(\hbar) = \xi \ \text{ and } \ y(\lambda) = \zeta, \tag{3.3}$$

where $\xi,\zeta$, are real constants, $\hbar = 0$, and $\lambda = 1$.

Integrating equation (3.1) with respect to $t$ from 0 to $t$ and using the Bc's given in equation (3.3), we get

$$y'(t) = \xi + \sum_{i=1}^{2^{k-1}m} a_i Q_{i,1}(t), \tag{3.4}$$

$$y(t) = t\xi + y(0) + \sum_{i=1}^{2^{k-1}m} a_i Q_{i,2}(t). \tag{3.5}$$

The value of $y(0)$ is given by

$$y(0) = \zeta - \xi - \sum_{i=1}^{2^{k-1}m} a_i C_{i,1}. \tag{3.6}$$

The approximate solution $y(t)$ can be written using equation (3.6), as follows

$$y(t) = \zeta + \xi(t-1) + \sum_{i=1}^{2^{k-1}m} a_i (Q_{i,2}(t) - C_{i,1}). \tag{3.7}$$

A $2^{k-1}m \times 2^{k-1}m$ linear or nonlinear system is produced by substituting the values of $y(t)$, $y'(t)$ and $y''(t)$ in the given differential equation and applying discretization using the collocation points (equation (3.7)). Now by solving this system, one may determine the Lucas coefficients $a_i$, $i = 1,2,\ldots,2^{k-1}m$. The approximated solution can be easily obtained by substituting the Lucas coefficients in equation (3.7). In our approach to error analysis, we apply the formula $E_{\max} = \max|\text{Exact solution} - \text{LWOMM solution}|$ to ascertain the maximum absolute error.

## 4. Lucas Wavelet Operational Matrix Method of Implementation

In this section, initially, we applied the LWOMM for the numerical solution of the differential equations to check the efficiency of the proposed method, later the projected technique is applied to analyse the squeeze film characteristics between a sphere and a flat plate.

**Test Problem 4.1.** First, we consider an ODE [5],

$$-((1+t)^2u')' + (1+t)(3+t)u = 3+t, \quad t \in [0,1]. \tag{4.1}$$

With the Bc's $u'(0) = 0$, and $u(1) = e + \frac{1}{2}$.

The exact solution of Test Problem 4.1 is $u(t) = e^t + \frac{1}{1+t}$.
Consider

$$u''(t) = \sum_{i=1}^{2^{k-1}m} a_i h_i(t). \tag{4.2}$$

Integrating equation (4.2) with respect to $t$ from 0 to $t$, and using the Bc, we get

$$u'(t) = \sum_{i=1}^{2^{k-1}m} a_i Q_{i,1}(t). \tag{4.3}$$

Once again, integrating equation (4.3) with respect to $t$ from 0 to $t$, and using the Bc we get

$$u(t) = u(0) + \sum_{i=1}^{2^{k-1}m} a_i Q_{i,2}(t). \tag{4.4}$$

The value of the unknown $u(0)$ is calculated as

$$u(0) = e + \frac{1}{2} - \sum_{i=1}^{2^{k-1}m} a_i C_{i,1}. \tag{4.5}$$

Using equation (4.5), the approximate solution $u(t)$ can be expressed as

$$u(t) = e + \frac{1}{2} + \sum_{i=1}^{2^{k-1}m} a_i [Q_{i,2}(t) - C_{i,1}]. \tag{4.6}$$

Substituting the equations (4.2), (4.3), and (4.6) in the given differential equation (4.1), and solving this equation, we get the Lucas coefficient matrix. Once again substituting this Lucas coefficient matrix in equation (4.6) we get the required solution of Test Problem 4.1. The obtained LWOMM solution is represented in Table 1 and Figure 2 with the FDM and analytic solution. Error analysis of LWOMM for different $N$ for Test Problem 4.1 in Table 2.

**Test Problem 4.2.** Secondly, consider an ODE [15],

$$u''(t) + u(t) + t = 0, \quad t \in (0,1) \tag{4.7}$$

subjected to Bc's $u(0) = u(1) = 0$. (4.8)

The exact solution of Test Problem 4.2 is $u(t) = \frac{\sin t}{\sin 1} - t$.

We obtain the LWOMM solution by the procedure as explained in Section 3. The comparison of the LWOMM solution with the FDM and analytic solution is presented in Table 3, and Figure 3. Error analysis is presented in Table 4 for different values of $N$.

**Lubrication Problem.** To analyse the SF characteristics the following non-dimensional parameters and variables are introduced,

$$\left.\begin{aligned} &\bar{R} = \frac{R}{r}, \quad \bar{P} = -\frac{Ph_0^2}{\mu r \frac{\partial h}{\partial t}}, \\ &\bar{h}_M = \frac{h_M}{h_0}, \quad \bar{L} = \frac{L}{h_0}, \\ &\gamma = \frac{h_0}{r}. \end{aligned}\right\} \tag{4.9}$$

Then the dimensionless modified Reynolds equation is represented as

$$\frac{1}{\bar{R}}\frac{\partial}{\partial \bar{R}}\left[\bar{F}(\bar{h},\bar{L})\bar{R}\frac{\partial \bar{P}}{\partial \bar{R}}\right] = -\frac{12}{\gamma}, \tag{4.10}$$

where

$$\bar{h} = \frac{h}{h_0} = \bar{h}_M + \frac{\bar{R}^2}{2\gamma}, \tag{4.11}$$

$$\bar{F}(\bar{h},\bar{L}) = \bar{h}^3 - 12\bar{L}^2\bar{h} + 24\bar{L}^3 \tanh\left(\frac{\bar{h}}{2\bar{L}}\right). \tag{4.12}$$

The Bc's for the current problem are as follows:

$$\bar{P} = 0 \text{ at } \bar{R} = 1 \quad \text{and} \quad \frac{d\bar{P}}{d\bar{R}} = 0 \text{ at } \bar{R} = 0. \tag{4.13}$$

Now, by applying the LWOMM as presented in Section 4, the obtained results are discussed in the next section.

**Load-Carrying Capability.** Through the integration of the film pressure exerted on the sphere, it is possible to calculate the load-carrying capacity.

$$w = 2\pi \int_0^\infty PR\, dR\,. \tag{4.14}$$

Presenting the non-dimensional quantity:

$$\bar{w} = -\frac{wh_0^2}{\mu r^3 \partial h/\partial t}. \tag{4.15}$$

The non-dimensional load-carrying capability ($\bar{w}$) can be expressed as

$$\bar{w} = \frac{6\pi}{\gamma}\int_0^1 \frac{\bar{R}^3}{\bar{F}(\bar{h},\bar{L})} d\bar{R}. \tag{4.16}$$

## 5. Results and Discussion

From Table 1, we can observe that the solution obtained by the LWOMM is well compared with the analytic solution.

**Table 1.** Numerical solution of Test Problem 4.1 for $N = 16$

| $t$ | FDM | LWOMM | Exact solution | Absolute error | |
|---|---|---|---|---|---|
| | | | | FDM | LWOMM |
| 0.03125 | 1.997214 | 2.001449 | 2.00144 | 4.226178E-3 | 8.664709E-6 |
| 0.09375 | 2.003926 | 2.012579 | 2.012571 | 8.644926E-3 | 7.990879E-6 |
| 0.15625 | 2.022778 | 2.033991 | 2.033983 | 1.120548E-2 | 7.550672E-6 |
| 0.21875 | 2.052856 | 2.06504 | 2.065033 | 1.217647E-2 | 7.307014E-6 |
| 0.28125 | 2.09353 | 2.105279 | 2.105273 | 1.174256E-2 | 6.709705E-6 |
| 0.34375 | 2.144386 | 2.154418 | 2.154412 | 1.002586E-2 | 5.821327E-6 |
| 0.40625 | 2.205188 | 2.212294 | 2.212289 | 7.100697E-3 | 5.086263E-6 |
| 0.46875 | 2.275843 | 2.278851 | 2.278847 | 3.003921E-3 | 4.477638E-6 |
| 0.53125 | 2.356376 | 2.354122 | 2.354119 | 2.257762E-3 | 3.838785E-6 |
| 0.59375 | 2.44692 | 2.43822 | 2.438217 | 8.702690E-3 | 3.171033E-6 |
| 0.65625 | 2.547695 | 2.531327 | 2.531324 | 1.637062E-2 | 2.586218E-6 |
| 0.71875 | 2.659005 | 2.633687 | 2.633685 | 2.532028E-2 | 2.072495E-6 |
| 0.78125 | 2.781232 | 2.745606 | 2.745604 | 3.562764E-2 | 1.567550E-6 |
| 0.84375 | 2.914827 | 2.867444 | 2.867443 | 4.738493E-2 | 1.070817E-6 |
| 0.90625 | 3.060314 | 2.999615 | 2.999614 | 6.070001E-2 | 6.158844E-7 |
| 0.96875 | 3.218282 | 3.142586 | 3.142586 | 7.569623E-2 | 1.981810E-7 |

As we can observe in Table 2, the LWOMM yields a solution to Test Problem 4.1 with a lesser error compared to the FDM.

**Table 2.** Error analysis of LWOMM for different $N$ for Test Problem 4.1

| $N$ | $E_{\max}$ | |
|---|---|---|
| | FDM | LWOMM |
| 4 | 2.860732E-1 | 1.551180E-3 |
| 8 | 1.485633E-1 | 1.097021E-3 |
| 12 | 1.002962E-1 | 1.925694E-5 |
| 16 | 7.569623E-2 | 8.664709E-6 |
| 20 | 6.078550E-2 | 1.671095E-7 |

From Figure 2, it is clear that the LWOMM solution is in good agreement with the exact solution.

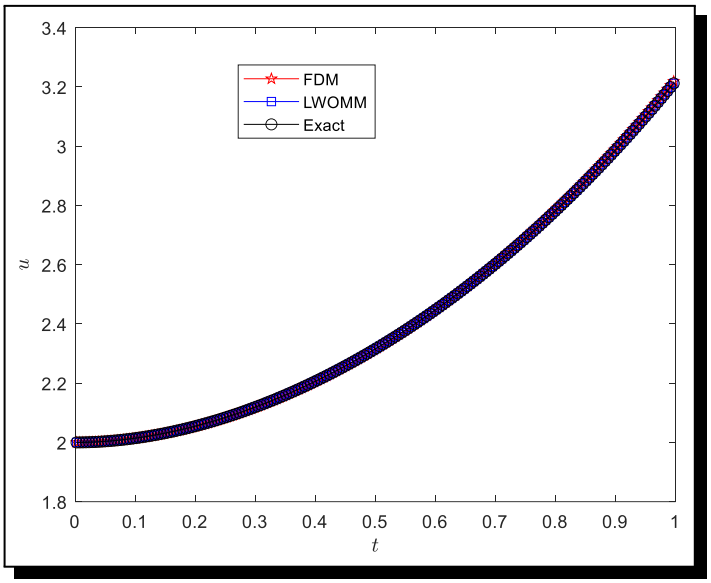


**Figure 2.** Compares the FDM, LWOMM, and Exact solutions for Test Problem 4.1 for $N = 192$

Table 3 illustrates that the solution derived from the LWOMM aligns favourably with the analytic solution.

**Table 3.** Numerical solution of Test Problem 4.2 for $N = 16$

| $t$ | FDM | LWOMM | Exact solution | Absolute error | |
|---|---|---|---|---|---|
| | | | | FDM | LWOMM |
| 0.03125 | 0 | 0.005881 | 0.005881 | 5.881302E-3 | 1.691362E-9 |
| 0.09375 | 0.012793 | 0.017499 | 0.017499 | 1.107372E-2 | 4.998277E-9 |
| 0.15625 | 0.025112 | 0.028682 | 0.028682 | 2.173797E-2 | 8.402164E-9 |
| 0.21875 | 0.036626 | 0.039143 | 0.039143 | 3.170696E-2 | 1.179606E-8 |
| 0.28125 | 0.047004 | 0.048597 | 0.048597 | 4.069761E-2 | 1.438050E-8 |
| 0.34375 | 0.055923 | 0.056763 | 0.056763 | 4.843064E-2 | 1.631969E-8 |
| 0.40625 | 0.063066 | 0.063365 | 0.063365 | 5.463172E-2 | 1.819076E-8 |
| 0.46875 | 0.068124 | 0.068133 | 0.068133 | 5.903248E-2 | 2.022503E-8 |
| 0.53125 | 0.070795 | 0.070805 | 0.070805 | 6.137159E-2 | 2.068143E-8 |
| 0.59375 | 0.07079 | 0.071125 | 0.071125 | 6.139577E-2 | 1.973171E-8 |
| 0.65625 | 0.067832 | 0.068849 | 0.068849 | 5.886079E-2 | 1.902768E-8 |
| 0.71875 | 0.061656 | 0.063742 | 0.063742 | 5.353241E-2 | 1.833347E-8 |
| 0.78125 | 0.052011 | 0.055579 | 0.055579 | 4.518729E-2 | 1.566681E-8 |
| 0.84375 | 0.038663 | 0.044149 | 0.044149 | 3.361391E-2 | 1.093206E-8 |
| 0.90625 | 0.021393 | 0.029251 | 0.029251 | 1.861333 E-2 | 6.397645E-9 |
| 0.96875 | 0 | 0.010700 | 0.010700 | 0 | 2.257702E-9 |

As shown in Table 4, the LWOMM provides a solution to Test Problem 4.2 with a smaller error in comparison to the FDM.

**Table 4.** Error analysis of LWOMM for different $N$ for Test Problem 4.2

| $N$ | $E_{\max}$ | |
|---|---|---|
| | FDM | LWOMM |
| 4 | 3.714494E-2 | 1.799038E-4 |
| 8 | 2.044284E-2 | 4.737460E-5 |
| 12 | 1.405261E-2 | 1.235764E-7 |
| 16 | 1.069963E-2 | 2.068143E-8 |
| 20 | 8.636873E-3 | 8.330973E-11 |

From Figure 3, it is clear that the LWOMM solution is in good agreement with the exact solution.

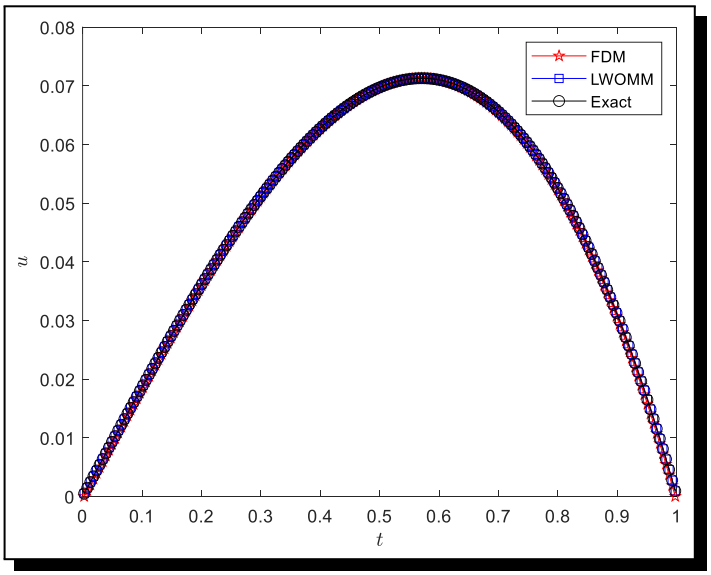


**Figure 3.** Comparison of the FDM, LWOMM, and exact solutions for Test Problem 4.2 for $N = 192$

**Pressure Distribution.** Figure 4 illustrates the non-dimensional film pressure ($\bar{P}$) produced by the SF action in relation to the non-dimensional radius ($\bar{R}$) for various values of the CS parameter ($\bar{L}$), with a non-dimensional minimum film height $\bar{h}_M = 0.3$ and $\gamma = 0.05$. The effects of CS lead to an increase in $\bar{P}$, particularly close to the location of the minimum film height. Figure 5 illustrates the non-dimensional maximum film pressure ($\bar{P}_{\max}$) in relation to the $\bar{h}_M$ for various values of $\bar{L}$. In comparison to the Newtonian lubricant scenario, the inclusion of CS effects results in a rise in the $\bar{P}_{\max}$. Additionally, the smaller the minimum SF height, the greater the impact of CS on the $\bar{P}_{\max}$.

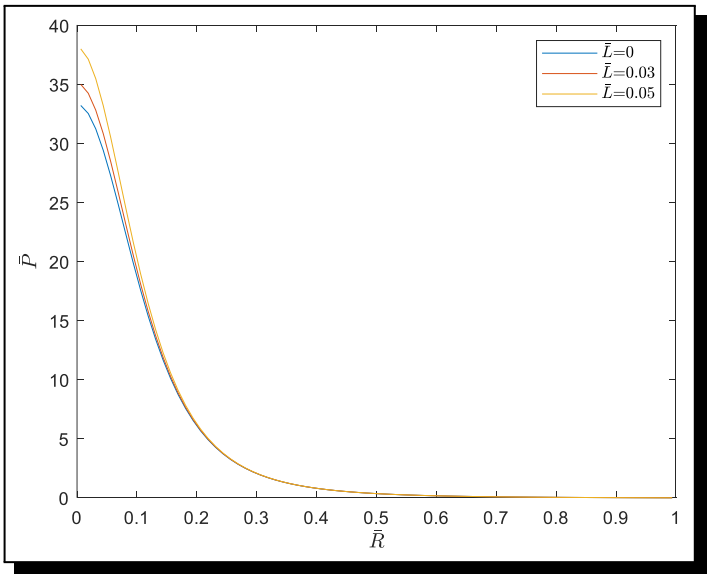


**Figure 4.** Non-dimensional pressure $\bar{P}$ for various $\bar{L}$ at $\bar{h}_M = 0.3$ as a function of $\bar{R}$

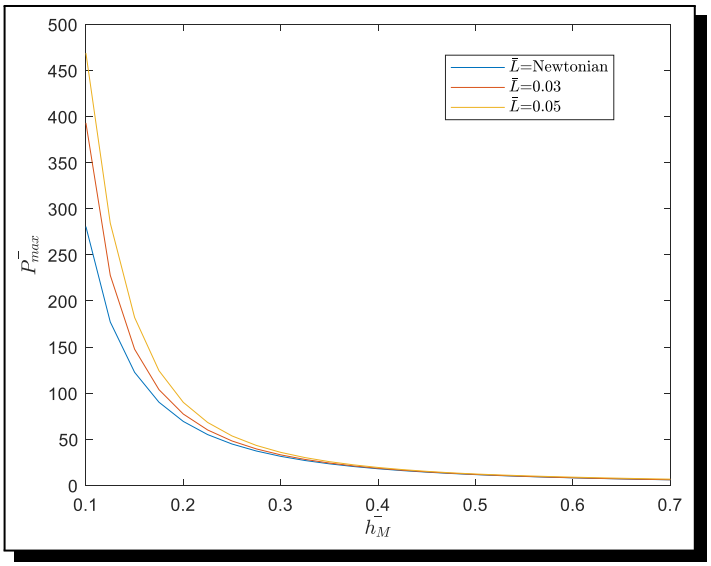


**Figure 5.** Fluctuation of $\bar{P}_{\max}$ relation to $\bar{h}_M$ for various $\bar{L}$

**Load-Carrying Capability.** Figure 6 illustrates the relationship between the $\bar{w}$ and the non-dimensional minimum film height ($\bar{h}_M$), considering different values of the CS parameter $\bar{L}$. The load-carrying capability is improved by the effects of CS in comparison to the Newtonian-lubricant case. The increment is greater when the value of $\bar{h}_M$ decreases or the value of $\bar{L}$ increases.

The examination of SF properties between a sphere and a flat plate, utilizing the CS fluid model, holds significant relevance for both physical and engineering contexts. The inclusion of couple stresses, reflecting the microstructural impacts of lubricants, leads to increased film pressure and improved load-carrying capability, in contrast to the traditional Newtonian fluid model. The enhancements lead to greater stability, efficiency, and durability of lubrication systems, essential for high-performance engineering applications like bearings, gears, turbines, and aerospace mechanisms.

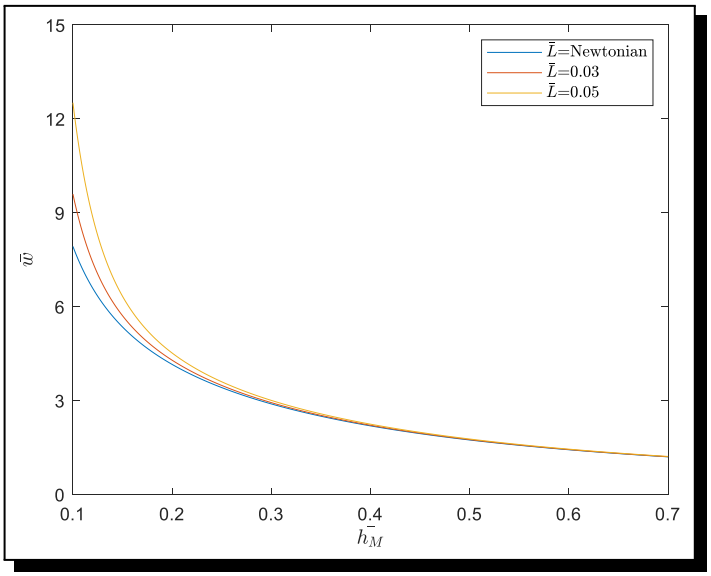


**Figure 6.** Variation of $\bar{w}$ in relation to $\bar{h}_M$ for various values of $\bar{L}$

## 6. Conclusion

The effects of CS on the SF motion between a sphere and a flat plate are examined using Stokes microcontinuum theory. The Stokes constitutive equations are used to construct the modified Reynolds equation for SF pressure, to account for CS effects. The SF features of the system are mostly influenced by the CS parameter. As the CS parameter approaches 0, the issue becomes the Newtonian-lubricant case. The ODE with an exact solution is regarded as the test problems, and the projected technique is implemented to resolve them. The findings obtained are compared with FDM. We found from the acquired solutions that the LWOMM solutions offer a good comparison to the exact solution for raising the value of $N$ with reduced error. The accuracy of the proposed technique allows for an extension to analyse the pressure distribution and load-carrying capability between a sphere and a flat plate by solving the corresponding non-dimensional modified Reynolds equation. The characteristics of SF in the sphere-plate system are notably influenced by the presence of CS. In contrast to the classical Newtonian-lubricant scenario, the influence of CS enhances both the pressure distribution and load carrying capability. Moreover, the quantitative effects become more significant when the system functions at lower SF height values.

## Acknowledgments

(1) We thank University Grants Commission (UGC), New Delhi, for supporting this work partially through UGC-SAP DRS-III for 2016-2021: F.510/3/DRS-III/2016 (SAP-I).

(2) Also thankful to the Council of Scientific and Industrial Research, New Delhi for Junior Research Fellowship: File No. 09/101(0060)/2020-EMR-I.

(3) Also thankful to the financial support from the Backward Welfare Department, Government of Karnataka.

## Competing Interests

The authors declare that they have no competing interests.

## Authors' Contributions

All the authors contributed significantly in writing this article. The authors read and approved the final manuscript.

## References


[1] T. Ariman, M. A. Turk and N. D. Sylvester, Microcontinuum fluid mechanics — A review, *International Journal of Engineering Science* **11**(8) (1973), 905 – 930, DOI: 10.1016/0020-7225(73)90038-4.

[2] T. V. Biradar, Squeeze film lubrication between porous parallel stepped plates with couple stress fluids, *Tribology Online* **8**(5) (2013), 278 – 284, DOI: 10.2474/trol.8.278.

[3] A. S. Burbidge and C. Servais, Squeeze flows of apparently lubricated thin films, *Journal of Non-Newtonian Fluid Mechanics* **124**(1-3) (2004), 115 – 127, DOI: 10.1016/j.jnnfm.2004.07.011.

[4] P. Chang and P. Piau, Haar wavelet matrices designation in numerical solution of ordinary differential equations, *IAENG International Journal of Mathematics* **38**(3) (2008), 5 pages, URL: https://www.iaeng.org/IJAM/issues_v38/issue_3/IJAM_38_3_11.pdf.

[5] A. H. Choudhury and R. K. Deka, Wavelet-Galerkin solutions of one dimensional elliptic problems, *Applied Mathematical Modelling* **34**(7) (2010), 1939 – 1951, DOI: 10.1016/j.apm.2009.10.011.

[6] H. Dehestani, Y. Ordokhani and M. Razzaghi, Combination of Lucas wavelets with Legendre–Gauss quadrature for fractional Fredholm–Volterra integro-differential equations, *Journal of Computational and Applied Mathematics* **382** (2021), 113070, DOI: 10.1016/j.cam.2020.113070.

[7] L. Fox, *Numerical Solution of Ordinary and Partial Differential Equations*, Pergamon Press, Inc., 520 pages (1962).

[8] C. F. Gerald and P. O. Wheatley, *Applied Numerical Analysis*, Pearson Education India, Boston, 609 pages (1999).

[9] P. S. Gupta and A. S. Gupta, Squeezing flow between parallel plates, *Wear* **45**(2) (1977), 177 – 185, DOI: 10.1016/0043-1648(77)90072-2.

[10] H. Hashimoto, Viscoelastic squeeze film characteristics with inertia effects between two parallel circular plates under sinusoidal motion, *ASME Journal of Tribology* **116**(1) (1994), 161 – 166, DOI: 10.1115/1.2927034.

[11] J. D. Jackson, A study of squeezing flow, *Applied Science Research, Section A* **11** (1963), 148 – 152, DOI: 10.1007/BF03184719.

[12] A. Kumar, The operational matrix method based on modified Lucas wavelets for the approximation solution of initial and boundary value problems, *International Journal of Applied and Computational Mathematics* **9** (2023), article number 147, DOI: 10.1007/s40819-023-01620-5.

[13] S. Kumbinarasaiah, M. P. Preetham and N. A. Shah, Analysis of magnetohydrodynamic laminar boundary layer flow, heat, and mass transfer of nanofluids on a moving surface with thermal radiation via Bernoulli wavelets technique, *Numerical Heat Transfer, Part B: Fundamentals* **86**(5) (2025), 1414 – 1437, DOI: 10.1080/10407790.2024.2312960.

**[14]** R.-F. Lu and J.-R. Lin, A theoretical study of combined effects of non-Newtonian rheology and viscosity-pressure dependence in the sphere-plate squeeze-film system, *Tribology International* **40**(1) (2007), 125 – 131, DOI: 10.1016/j.triboint.2006.03.004.

**[15]** N. Mai-Duy and T. Tran-Cong, An integrated-RBF technique based on Galerkin formulation for elliptic differential equations, *Engineering Analysis with Boundary Elements* **33**(2) (2009), 191 – 199, DOI: 10.1016/j.enganabound.2008.05.001.

**[16]** V. Mehandiratta, M. Mehra and G. Leugering, An approach based on Haar wavelet for the approximation of fractional calculus with application to initial and boundary value problems, *Mathematical Methods in the Applied Sciences* **44**(4) (2021), 3195 – 3213, DOI: 10.1002/mma.6800.

**[17]** N. B. Naduvinamani, P. S. Hiremath and G. Gurubasavaraj, Static and dynamic behaviour of squeeze-film lubrication of narrow porous journal bearings with coupled stress fluid, *Proceedings of the Institution of Mechanical Engineers, Part J: Journal of Engineering Tribology* **215**(1) (2001), 45 – 62, DOI: 10.1243/1350650011541738.

**[18]** O. Oruç, A new algorithm based on Lucas polynomials for approximate solution of 1D and 2D nonlinear generalized Benjamin–Bona–Mahony–Burgers equation, *Computers & Mathematics with Applications* **74**(12) (2017), 3042 – 3057, DOI: 10.1016/j.camwa.2017.07.046.

**[19]** P. Rahimkhani, Y. Ordokhani and E. Babolian, Müntz-Legendre wavelet operational matrix of fractional-order integration and its applications for solving the fractional pantograph differential equations, *Numerical Algorithms* **77**(4) (2018), 1283 – 1305, DOI: 10.1007/s11075-017-0363-4.

**[20]** J. N. Reddy, *Introduction to Finite Element Method*, McGraw-Hill Education, 784 pages (2006).

**[21]** S. C. Shiralashetti, A. M. Sangolli and P. R. Badiger, Daubechies wavelet multigrid method for accurate solution of typical differential equations arising in hydrodynamic lubrication theory, *Indian Journal of Science and Technology* **18**(6) (2025), 430 – 442, DOI: 10.17485/IJST/v18i6.2416.

**[22]** S. C. Shiralashetti, V. R. Pala and S. I. Hanaji, Jacobi wavelet integration operational matrix method for the numerical solution of laminar nanofluid flow problem, *International Journal of Ambient Energy* **46**(1) (2025), Article: 2458178, DOI: 10.1080/01430750.2025.2458178.

**[23]** V. K. Stokes, Couple stresses in fluids, *Physics of Fluids* **9**(9) (1966), 1709 – 1715, DOI: 10.1063/1.1761925.

**[24]** C. Torrence and G. P. Compo, A practical guide to wavelet analysis, *Bulletin of the American Meteorological Society* **79**(1) (1998), 61 – 78, DOI: 10.1175/1520-0477(1998)079<0061:APGTWA>2.0.CO;2.